Recycling a carbon fiber-reinforced polyamide through 3D printing: a mechanical and physicochemical analysis

Composites Part B 294 (2025) 112147

Contents lists available at ScienceDirect

Composites Part B

journal homepage: www.elsevier.com/locate/compositesb

Recycling a carbon fiber-reinforced polyamide through 3D printing: A mechanical and physicochemical analysis

Francesco Bandinelli [a,*], Edoardo Tito [b], Emmanuele Parisi [b], Lorenzo Peroni [a], Martina Scapin [a]

[a] Politecnico di Torino, Department of Mechanical and Aerospace Engineering, Corso Duca degli Abruzzi, 24, 10129, Turin, Italy
[b] Politecnico di Torino, Department of Applied Science and Technology, Corso Duca degli Abruzzi, 24, 10129, Turin, Italy

ARTICLE INFO

Handling Editor: Prof. Ole Thomsen

ABSTRACT

Plastic waste is one of the major challenges of our times. With a global recycling rate of only 9 % and a continuous rise in plastic production, it is crucial to explore solutions to mitigate this problem. Mechanical recycling of plastic materials is one of the most accessible and widely used methods to recover thermoplastic polymers. In this study, a short-carbon-fiber-reinforced polyamide is mechanically recycled and recovered through Fused Granular Fabrication (FGF) 3D printing to print new parts. Chemical and mechanical analyses are conducted to investigate possible molecular alterations due to the recycling process, evaluating the effectiveness of the simplest recovery system. Additionally, FGF and Fused Filament Fabrication (FFF) are compared to assess any significant difference between the two technological solutions. Chemical analyses show no substantial difference in the chemical and physical properties of pristine and recycled material. However, micro-CT scans and tensile tests show notable differences between FGF and FFF technologies in microstructure and mechanical properties. Recycled specimens result 24 % and 6 % denser than FFF and FGF pristine respectively (having the same volume). This results in a maximum increase in stiffness (up to 43 %) and ultimate strength (up to 20 %) for recycled dogbone specimens. Besides minor microstructural aspects, no relevant differences are found between pristine and recycled material printed using FGF. A case study on sandwich cores is presented showing the feasibility of the recycling process. Due to its higher density, the recycled core performs 26 % lower in energy absorption when compared to pristine ones at the same weight.

1. Introduction

Plastic waste management is one of the most pressing challenges of our time, demanding immediate and decisive action. In 2019 global plastics production reached 460 Mt, with an estimated annual waste of approximately 353 Mt [1]. In the same year, the waste was managed as follows: 9 % was recycled, 19 % incinerated, 22 % mismanaged, and 49 % landfilled, making the plastic market practically linear [2]. In the baseline scenario, plastics production is projected to almost triple by 2060, while the recycling rate is expected to increase only to 17 % [1]. To address this issue, it is necessary to re-shape the plastic market to a circular model, reducing overall production and increasing the fraction of reuse and recycling as well as developing alternatives [3–5]. Especially highly technological polymers, such as fiber-reinforced ones, are currently landfilled due to active recycling policies. In this context, it is important to establish a viable recycling path to focus on the recovery of high value plastic streams. Additive manufacturing represents a viable option to deal with recycled polymers, potentially increasing the fraction of plastics production through mechanical recycling [6–8]. In recent years, an increasing number of studies dealt with the 3D printing of recycled polymers, evaluating the process and their mechanical properties [9–19]. The results of these studies demonstrated that recycled thermoplastic polymers can be effectively processed and remanufactured by 3D printing.

Romani et al. [10] investigated the mechanical properties of PLA subjected to multiple recycling processes using Fused Granular Fabrication (FGF) with shredded material from previous cycles. They found that PLA loses mechanical strength with each cycle and experiences a reduction in molecular weight. Similar results are reported by Sanchez et al. [11], although they found that multiple recycling processes enhanced PLA flowability, reducing air pores and improving inter-layer adhesion. A common result in studies regarding the 3D printing of

* Corresponding author.
E-mail address: francesco.bandinelli@polito.it (F. Bandinelli).

https://doi.org/10.1016/j.compositesb.2025.112147
Received 19 November 2024; Received in revised form 8 January 2025; Accepted 14 January 2025
Available online 16 January 2025

fiber-reinforced recycled polymers is the reduction of fiber length and subsequent mechanical performances [9,14,16,18]. For instance, Wu et al. [16] observed relevant fiber length reduction when recycling and printing carbon fiber with a PA6 matrix, leading to a marked decrease in mechanical properties. They also improved the latter by hot pressing the specimens, reducing typical porosities of highly filled 3D-printed polymers. Su et al. [18] conducted a similar study, reporting a total reduction of 60 % in fiber length during filament production and 3D printing. Rigon et al. [9] compared the mechanical properties of glass fiber-reinforced recycled polypropylene produced by Pellet Additive Manufacturing (PAM) with those of virgin injection molded material. They found that the recycling process shortened the glass fibers, thus reducing the mechanical properties of the recycled 3D-printed material. They also observed chemical degradation of the polymeric matrix.

Among additive manufacturing technologies, FGF allows 3D printing directly from recycled flakes produced by shredding plastics [9,20–22]. This 3D printing technology resembles the conventional Fused Filament Fabrication (FFF) technique but requires pellets or flakes as feedstock. This not only simplifies some issues related to spool change and filament breakage but also reduces costs while preserving final results [20, 23–26]. In addition, highly fiber-filled materials are more difficult to be filamented and suffer from fiber breaking, hence FGF represents an attractive option for this class of composites.

Despite recent efforts to evaluate the feasibility of recycling polymers via additive manufacturing, the coverage of various materials is still limited. Typically, recycled polymers are re-extruded to produce filaments for 3D printing, while more direct usage of recycled waste has not been extensively investigated. This approach is particularly beneficial to the reduction of equipment, emissions, and lead time in recycling operations associated with additive manufacturing processes. Furthermore, to the best of the authors' knowledge, comprehensive studies on the recycling process via 3D printing and its application to functional components are lacking. This leaves the effectiveness of the whole recycling process underexplored. Knowledge of the mechanical recycling process is crucial for encouraging the spread of these manufacturing processes as a tool for the circularization of the plastics market. Nowadays, most of the studies are limited to the evaluation of the recycling process and/or mechanical properties of standard specimens, failing to address possible engineering applications. Furthermore, to the best of the author's knowledge, no study on recycled polymers via 3D printing has combined the mechanical characterization to the microstructure observed through micro-CT scans before testing.

The present work focuses on the mechanical performances of a short carbon fiber-reinforced (10 wt%) polyamide (PA12). The choice for this material is motivated by the need to address the challenge of recycling high-value materials that are landfilled due to current policies (such as polyamides). The establishment of a feasible recycling process could promote efforts to improve regulations and reduce waste. The comparison is developed on two different levels. First, FFF and FGF printing techniques are compared using the same feedstock to assess the main differences introduced by the different technological processes. Second, printed parts of the same material with different usage histories are shredded into flakes, which are then used as feedstock for new FGF prints. Tensile tests and physicochemical analyses are conducted to evaluate and explain possible significant changes in the mechanical performance of the recycled material. Micro-CT scans, as well as Differential Scanning Calorimetry (DSC), Thermogravimetric Analysis (TGA) and Fourier Transformed Infrared (FTIR) analysis are employed to deeply investigate multiple aspects of the recycling process. The entire recycling process is illustrated in Fig. 1. Finally, a case study is proposed: recycled material is used to 3D print a stiffener core for aluminum sandwich panels. The parts are examined to assess the quality of the 3D printing process and bending tests are conducted to evaluate their performances as functional components. This case study is chosen to demonstrate the efficiency of 3D-printed lattice structures as lightweight components, which are advantageous for reducing weight while providing high specific mechanical properties. Furthermore, the present work is one of the few works presenting a multi-scale analysis of the mechanical properties and functionality of recycled 3D-printed structural parts.

2. Materials and methods

2.1. Materials

The material analyzed in this work is Nylforce Carbon, a short fiber-reinforced polymer consisting of a PA12 matrix with 10 wt% short carbon fibers, produced by FiberForce (Treviso, Italy). The material is available in filament form (1.75 and 2.85 mm diameter) and is designed for FFF 3D printing. In this study, the same material is used in three different forms: pristine filament, pristine pellets (obtained from manually cutting the filament), and shredded recycled flakes. The latter two forms are illustrated in Fig. 2a and b. The recycled material is derived from old prints with different usage histories (temperature, humidity, chemical contamination, etc.), thus representing a wide spectrum of potential alterations. The 3D-printed parts are shredded using an industrial shredder (PiovanGroup, Santa Maria di Sala, Italy) and sifted to remove flakes larger than 5 mm, preventing clogging

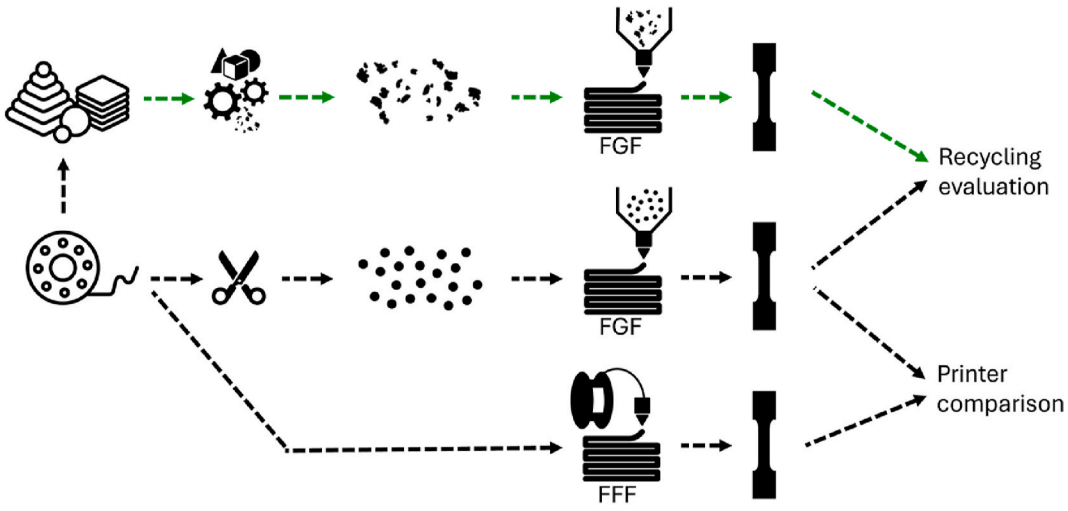

Fig. 1. Scheme of the printing and testing analysis proposed. Dashed green lines indicate the recycling path. (For interpretation of the references to colour in this figure legend, the reader is referred to the Web version of this article.)

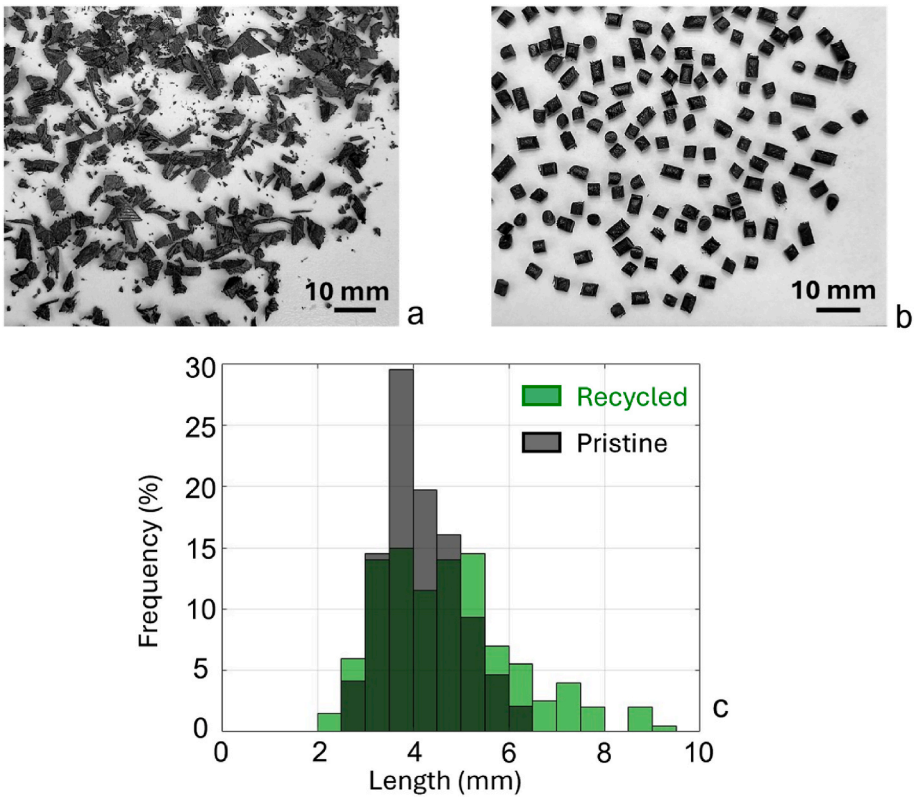

Fig. 2. Recycled material (a), pellets (b) and representative size distribution (c).

during the FGF printing [27]. The estimated cost of the shredding is 0.09 €/kg based on the machine consumption and cost of electricity. No treatments or washing processes are performed on the recycled material, investigating the most direct recycling path that minimizes emissions and costs. The size distribution of both flakes and pellets was evaluated using ImageJ software with the results shown in the graph in Fig. 2. Fig. 2a shows the recycled material and Fig. 2b shows pellets cut from the pristine filament. Fig. 2c shows a representative size distribution and related occurrence for flakes and pellets.

2.2. Preliminary chemical analyses

A thermogravimetric analysis is conducted using a Mettler Toledo SDTA851 (Mettler Toledo, Columbus, United States). Approximately 30 mg of the samples analyzed is placed in a 150 μL alumina crucible. The temperature program starts at 25 °C and increases to 600 °C with a heating ramp of 10 °C/min under an argon flow of 50 mL/min. Each analysis is performed in duplicate and the resulting average is plotted, along with the confidence intervals. The Initial Decomposition Temperature (IDT) is determined as the temperature at which a mass loss of 5 % is observed.

To evaluate melting temperatures and compare the material in the filament and recycled forms, Differential Scanning Calorimetry (DSC) analysis is performed using a Hitachi Nexta DSC200 (Hitachi, Tokyo, Japan). Approximately 9 mg of the samples analyzed are placed in a 40 μL aluminum pan. The pans are sealed with a press and isolated from the external atmosphere of the DSC furnace. The measurements were carried out using heating and cooling rates of 10°/min ranging from 25 °C to 300 °C with a continuous air gas flow at 50 ml/min. As a reference, an empty aluminum pan was used. The heating rate is chosen to mimic the heating rate of the printing process, which is calculated by measuring the initial and final temperature by thermocouples and the time taken for the feeding material to be extruded. Each measurement consists of two heating and cooling cycles of the same specimen, performed in duplicate. It is important to note that the cooling phase in DSC analysis does not accurately represent the actual cooling rate of the printing process, as the latter occurs within seconds. The degree of crystallinity (χ_c) was calculated using Eq. (1), where ΔH_m represents the melting enthalpy experimentally obtained during the first heating cycle, ω is the fraction of carbon fibers evaluated by TGA, and ΔH_m^0 is the reference melting enthalpy (209.3 J/g) for crystalline PA12 [28–30].

$$\chi_c\ (\%) = (\Delta H_m\ /\ (\Delta H_m^0\ (1-\omega))) \bullet 100 \quad (1)$$

Fourier transform infrared spectroscopy (ATR- FTIR) was used to investigate the chemical structure of the samples. FTIR spectra were collected using a Bruker Tensor 27 FTIR spectrometer (Bruker Optics, Billerica, United States) equipped with an Attenuated Total Reflection (ATR) accessory, covering a wavenumber between 4000 and 400 cm^{-1} with a resolution of 1 cm^{-1}. The analysis was conducted at room temperature by pressing the sample tightly against the crystal surface. Molecular vibrations were identified based on the literature [31–35].

2.3. 3D printing

Two different printers are used to realize test specimens: the Ultimaker S2+ Connect (Ultimaker B.V., Utrecht, NL), a common FFF printer, and PioCreat G5 Pro (PioCreat, Shenzhen, China), an FGF printer. The first printer is used to print the filament of Nylforce Carbon, while the second one is used to print both recycled and pelletized materials. Fig. 3 shows the scheme of the printing head of the FGF printer, providing details about the internal structure.

Printing parameters are the same for the two printers as well as for the different material forms. The nozzle temperature is set to 230 °C, the bed temperature to 50 °C, the printing speed to 30 mm/s, and the fan is switched off. The printing parameters are chosen based on previous studies by the authors. The nozzles used for the printing jobs have a ruby tip with a 0.8 mm diameter, which is durable, minimizes fiber breakage [16], and avoids clogging issues [23]. It is important to note that, for

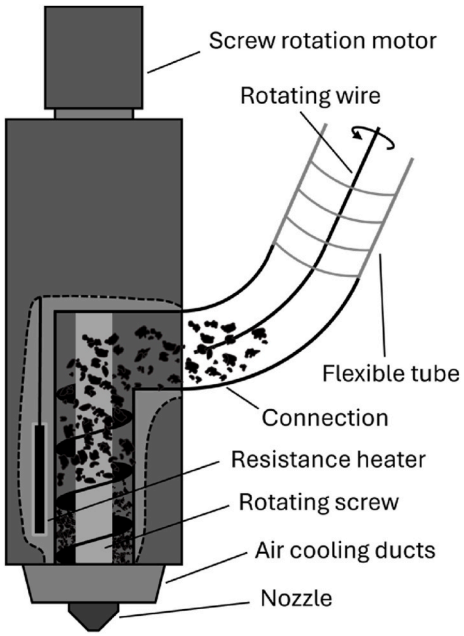

Fig. 3. Scheme of the FGF printer head (side view).

both printers, the temperature set for the printing process does not reflect the actual temperatures achieved during printing. The temperature of the nozzle and that of the extruded filament are monitored using thermocouples and an infrared camera Optris Pi (Optris, Berlin, Germany), revealing significant differences. For the FGF printer, a set temperature of 260 °C results in an actual printing temperature of 230 °C, while for the FFF printer, the same setting yields an actual temperature of 245 °C. Consequently, multiple printing tests are conducted to establish a consistent printing temperature of 230 °C for both printers. Additionally, modifications are made to the FGF 3D printer to adapt the system to the feedstock of the recycled material. Recycled flakes exhibit increased friction inside the feeding system. To address this, the entrance to the collection chamber was redesigned. In this trait, the feeding material comes from the collection tube and changes its path from almost vertical to horizontal, so it is subjected to clogging. The new connection piece is 3D-printed and smooths the movement of the recycled flakes, as shown in Fig. 3. In addition, an electric motor connected to a thick wire is installed at the top of the printer as a bridge-breaking system. This motor operates at a constant rotation speed during printing, effectively preventing clogging.

2.4. Specimens

In this study, two specimen types are chosen to study the longitudinal (parallel to the deposition direction) and transverse (along the vertical building direction) properties of the printed material. This choice is motivated by the significant anisotropy that characterizes 3D-printed material, necessitating an examination of how printing direction influences mechanical properties [36–38]. The first specimen type is a dogbone specimen, and the second is a tubular tensile specimen. The aim is to compare pristine and recycled materials under two extreme cases typical of 3D printing: maximum achievable strength and layer adhesion. This comparison is facilitated by ensuring that the raster angle does not influence results, shifting the focus from the microstructure to the actual material properties. The dogbone specimen is printed with a 0° raster angle, meaning all the deposited filaments run parallel to the longitudinal direction. Generally, in this configuration, the nozzle path is such that the fillets are inevitably characterized by defects, which may represent failure points, so the properties are underestimated [39,40]. To overcome this limit, the authors propose a modified G-code that makes the nozzle travel along a single path, without interruptions or directional changes in critical parts of the specimen. As shown in Fig. 4 (left image), this printing path (blue trajectory in Fig. 4) realizes a unidirectional gauge length and deviates to create fillets without abrupt movements, ensuring that no defects are introduced in these regions and failures are observed only in the effective gauge length. The material flow is adjusted to increase at the specimen heads compensating for the increased distance of the printed lines.

Conversely, tubular specimens (right image in Fig. 4) are characterized by a single pass of the nozzle in circular paths, allowing for focused evaluation of layer adhesion. The choice of a tubular specimen is motivated by the ease of printing, as vertical bulk printing often results in defects and inappropriate layer cooling [21]. Moreover, many 3D-printed lightweight structures are made of thin walls, making tubular specimens a suitable choice to analyze these properties.

Micro-CT scans are conducted on the FFF, pellet FGF, and recycled FGF for both tubular and dogbone specimens to assess the microstructure of the printed material. Fig. 5 displays micro-CT scan images of the three tubular specimens analyzed, while Fig. 6 displays those of dogbone specimens, revealing notable microstructural differences. The FFF specimens are characterized by numerous air pores, while FGF specimens appear significantly more compact. This difference is expected, as FGF printing involves a larger volume of fused material that is pressurized by a rotating screw, effectively reducing air voids [23]. In contrast, FFF printing pushes the filament through a small heated region and the same pressure buildup does not occur. The recycled FGF

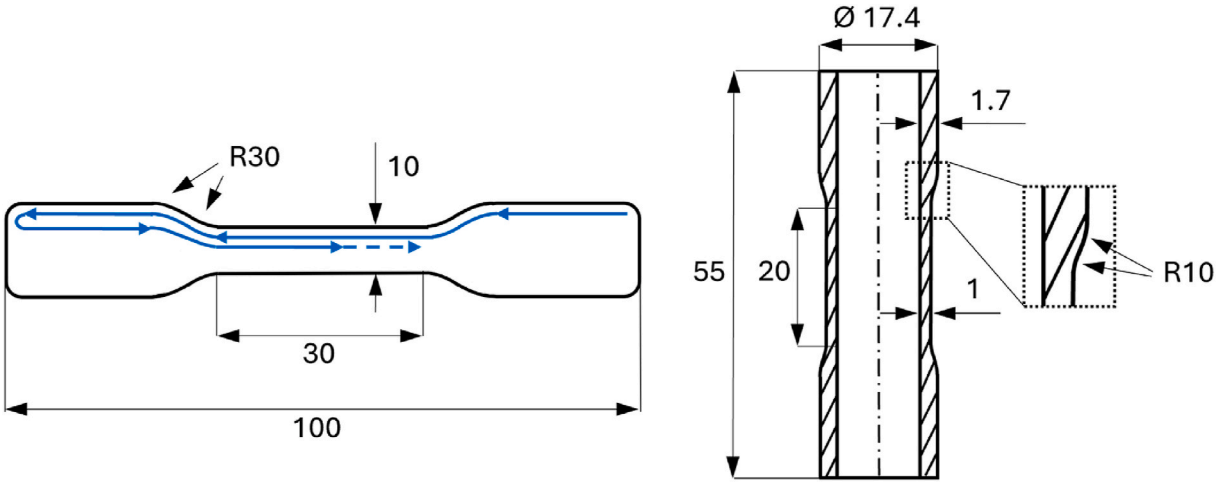

Fig. 4. Specimens used for tensile tests. Dimensions are reported in millimeters.

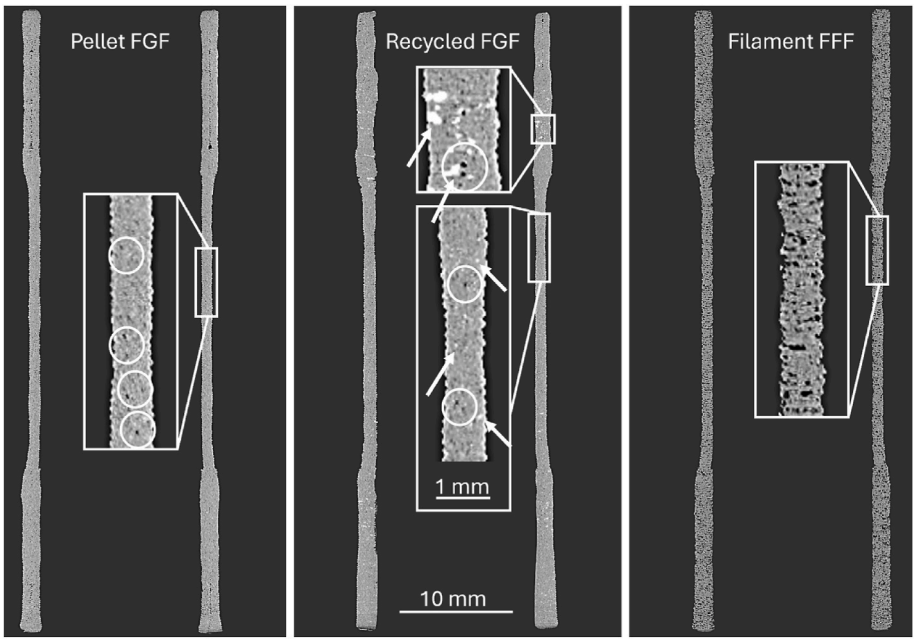

Fig. 5. Micro-CT scans of the tubular specimens. Details of the walls are shown (white boxes). White arrows indicate higher-density inclusions (bright points), while white circles indicate the presence of air pores.

specimens show some higher-density inclusions, probably due to their previous operational life. From the geometrical point of view, the pellet FGF specimens show a more constant cross-section compared to their recycled counterparts. Flow variations during the printing process are caused by the non-uniformities in the feeding system of the FGF printer, due to size differences of the particles. This effect is particularly evident in the recycled prints, where the cross-section is less uniform. FFF printing, although introducing a lot of air pores, results in a more precise geometry. Another important observation is the differing concentrations of air pores in FFF tubular and dogbone specimens. This difference

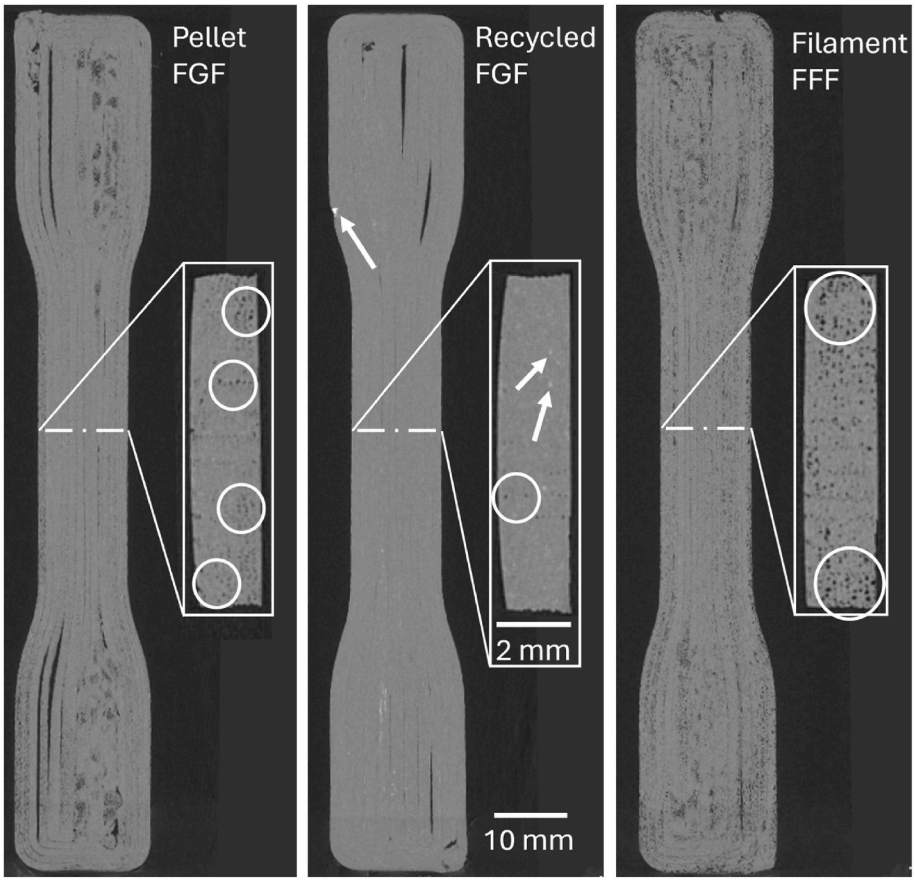

Fig. 6. Micro-CT scans of the dogbone specimens. Details of the cross sections are shown (white boxes). White arrows indicate higher-density inclusions (bright points), while white circles indicate the presence of air pores.

suggests that the air pores concentration does not only depend on the printing process but also on the geometry realized. In the tubular specimens, the deposited material does not encounter obstacles since the walls are realized by a single pass and there is no pressure buildup. Consequently, the filament expands freely when exiting the nozzle and the material is not further compacted. In contrast, when printing dogbone specimens, multiple nozzle passes are used and the effect is to confine the deposition of fused material, possibly limiting the formation of air voids [41]. Dogbone specimens are characterized by notable voids in the head region; however, this does not compromise the results of the tensile tests. The material flow is subjected to fluctuations and tuning it throughout the entire G-code is a challenging task, so the authors focused on the satisfactory realization of the gauge lengths. Tubular specimens do not experience the same defects due to their simpler nozzle path. Each layer is characterized by a single or double circumference for the gauge length and head, respectively, and no tuning of the material flow is required, differently from the case of dogbone specimens.

It is important to focus on the significance of thin-walled specimens for the mechanical characterization of 3D-printed materials. With vertically aligned dogbone specimens (printed with their longitudinal axis aligned with the building direction), the relevant difference in terms of microstructure would not be observable and the characterization would be incomplete or misrepresented. Most 3D-printed parts are made by thin walls and the characterization via bulk specimens could be not representative of the real case. The influence of wall thickness on the mechanical properties of 3D-printed structures has been only studied in a few works, denoting the need for future in-depth analyses [42]. Lastly, measurements of the cross-section area of dogbone specimens are repeated across the width to account for the roundness of the base and then averaged. For tubular specimens, thickness and diameters are measured after the tests along the height far from the fracture surface to exclude the effects of plastic deformation (although very limited).

2.5. Tensile tests

Tensile tests are conducted on an electromechanical universal testing machine Zwick-Z005 (ZwickRoell GmbH & Co. KG, Ulm, Denmark), equipped with a 5 kN load cell. For both specimen types, an engineering strain rate of 10^{-2} s^{-1} is applied for quasi-static properties evaluation. Video recording during the tests is performed with a PixeLINK PL-B777 camera with a 5 MP resolution (PixeLINK, Ottawa, Canada) and equipped with a Tokina Macro 100 F2.8 D camera lens (Kenko Tokina Co. Ltd, Tokyo, Japan). Image analysis is subsequently conducted for strain measurement and failure analysis.

2.6. Case study

A case study is analyzed to assess the reliability of the printing process using recycled materials and to study the performance of a recycled 3D-printed component. In this study, a sandwich panel core is fabricated using FGF with recycled PA12 with 10 % wt. of short carbon fibers, with the same printing parameters as described in section 2.4. The cores are bonded to 1.2 mm thick aluminum plates (Al5754–H32) using epoxydic adhesive Loctite EA 9514 (Henkel, Düsseldorf, Germany), obtaining a lightweight and stiff component. The excess of 3D-printed material is removed until reaching the aluminum panel width of 50 mm. Bending tests are conducted to evaluate the properties of the structure and the feasibility of employing recycled material as a core for sandwich components. Fig. 7 shows a scheme of the bending test on a sandwich specimen and details of the printed cores.

All the printed cores are realized by a “cubic” cellular structure realized by the slicer Cura (version 5.7.0), in which the elementary cell is represented by a closed cube with a vertically oriented diagonal. This cellular structure has demonstrated exceptional efficiency in energy absorption, withstanding high loads and significant plastic deformation [43]. The recycled printed cores are printed on the PioCreat G5 Pro using a 0.8 mm ruby nozzle with a spacing of 15 mm between printed lines. The overall density of the core is set to 320 g/l, to be comparable with other technological solutions, such as aluminum foams. Due to the different densities of recycled FGF and pristine FFF materials, the internal structure of the cores must be adjusted to achieve equivalent component weight. To this end, FFF-printed cores are modified by increasing the cell density (Fig. 7a) or thickening the walls (Fig. 7c).

The 3-point bending tests are conducted on the sandwich specimens using an electromechanical universal testing machine Zwick Z-100 (ZwickRoell GmbH &Co. KG, Ulm, Denmark). The testing speed is set to 25 mm/min, with a maximum displacement of 35 mm. Video recordings are conducted for failure analysis.

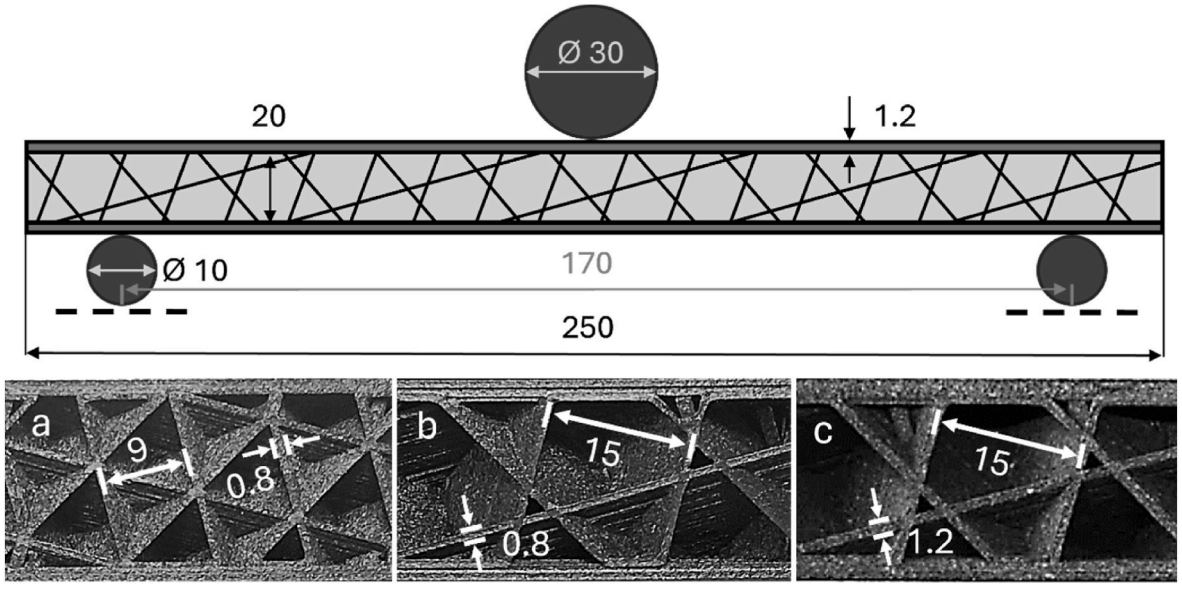

Fig. 7. Scheme of the bending test on the sandwich. Details of FFF small cells structure (a), FGF recycled structure (b), and FFF big cells structure (c). Dimensions are reported in millimeters.

3. Results and discussion

3.1. Chemical analysis results

Fig. 8 (left) shows the thermal behavior of both the pristine polymer and the recycled one. Interestingly, no significant differences are observed between the two samples. TGA results are presented in terms of residual mass percentage (solid lines) and mass variation over time (dashed lines) with respect to temperature. The green and black curves represent the recycled and pristine material results, respectively. The right image shows the graph of the FTIR analysis on pristine and recycled material. Wavelengths corresponding to relevant peaks are highlighted through black arrows. The IDT is 428 °C, with the mass loss corresponding to a single peak centered at 462 °C, indicative of the PA12 volatilization. This value is similar to that observed in similar analyses of PA12 samples [44]. At 600 °C, a residual mass of 8.4 ± 0.6 % is recorded. This value can be attributed to the carbon fibers present in the polymer.

To observe any differences in molecular bondings and chemical structure, ATR-FTIR is performed on the pristine and recycled material, and the resulting spectra are depicted in Fig. 8 (right). No significant differences are observed between the two samples. The main peaks are registered at 3290 cm^{-1} (N–H stretching), 2918 and 2815 cm^{-1} (C–H stretching), 1637 cm^{-1} (amide I C═O stretching), 1549 cm^{-1} (amide II, C–N stretching plus C═O in-plane bending), 1466 cm^{-1} (C–H bending), and 719 cm^{-1} (amide IV N–H out-of-plane bending). All these signals belong to the chemical structure of PA12, without any sensitive variations due to possible degradation. Moreover, the intense peak observed at 719 cm^{-1} is particularly notable, as it indicates that the crystalline phase present in the samples is the γ-phase (or γ′-phase) rather than the α-phase [32]. The γ-phase forms after melt crystallization at ambient temperature and pressure; it is the most stable phase and typically exhibits the highest tensile strength, elastic modulus, and elongation [32,45]. As the FTIR spectra were similar between the two samples, it is reasonable to assume that during the extrusion process of the recycled sample, the same crystalline structure formed as in the pristine material.

A study by Nur-a-Tomal et al. [46] on multiple recycling of PA12 evidenced analogous results in terms of FTIR analysis. Over four recycling processes no relevant difference was observed in terms of molecular structure. It is then reasonable to conclude that PA12 is not subjected to major effects in terms of molecular bonds and functional groups due to multiple mechanical recycling processes.

Fig. 9 exhibits the DSC heating and cooling curves of the pristine and recycled material. The DSC graph's dashed curves indicate each run's second heating cycle. The dashed vertical line in the DSC graph indicates the printing temperature of the specimens (T_p). The DSC data are summarized in Table 1, with standard deviations inside the brackets. A total of 2 samples of each material are used for the DSC analysis. Both samples show an exothermic hump in the first heating cycle before they start melting, which can be accounted for a reordering of polymer chains into a crystalline phase promoted by the increased temperature [47]. However, no shoulder at lower temperatures is observed, confirming the absence of the crystalline α-phase in both samples [32]. There is a small difference in melting temperature (T_m) between the two samples, with the pristine material having a slightly higher melting point than the recycled one (177.0 °C vs. 175.3 °C). This slight difference may be explained by the samples' size variations. Specifically, to fit the DSC crucible, smaller pieces were used for both samples, resulting in the recycled samples being smaller than the pristine ones, which could explain the slightly lower melting temperature of the recycled material due to a reduced internal thermal gradient. Despite this temperature difference, the variations in melting enthalpies (ΔH_m) fall within the experimental margin of error (47.8 ± 0.6 J/g and 49.4 ± 2.4), suggesting a consistent degree of crystallinity (χ_c) across both samples (25.0 ± 0.5 % and 25.7 ± 1.4 %). This consistency is noteworthy, considering that the recycled sample has undergone an additional extrusion cycle. Regarding crystallization, the temperature peak (T_c) is not different between the samples (153.4 ± 0.8 °C and 153.8 ± 0.1 °C), meaning that there is no nucleating effect on the recycled material. However, important differences in the crystallization enthalpy are registered. Specifically, the pristine material showed an enthalpy value of 47.2 J/g while the recycled one registered a much higher value of 60.0 J/g. A possible explanation for this difference could be found in post-crystallization phenomena, which lead to condensation between terminal groups when exposing polymers to high temperatures. This phenomenon is more important for new unstressed polymers [28,48], and leads to increased Mw, reduced mobility, and ultimately decreased crystallization enthalpy (ΔH_c) [28]. The post-crystallization could be particularly pronounced in this study due to the high temperature of the DSC cycle (300 °C) compared to the extrusion temperature (230 °C). Consequently, the pristine material, without any prior thermal history, may be more affected by this phenomenon, while the recycled material, having undergone extrusion and prior use, appears more resistant to high temperatures. In the second heating cycle, a shoulder appears in the melting peak of both samples (Fig. 9), indicating a melting-recrystallization process specific to the α-phase [32]. This suggests that the cooling cycle performed during the DSC analysis does not accurately represent the conditions during extrusion, as the in-printing cooling happens in the order of seconds. Identical results were obtained by Wang et al. [49] for carbon fiber-filled PA12, while investigating the effect of the recycling process of both polymeric matrix and

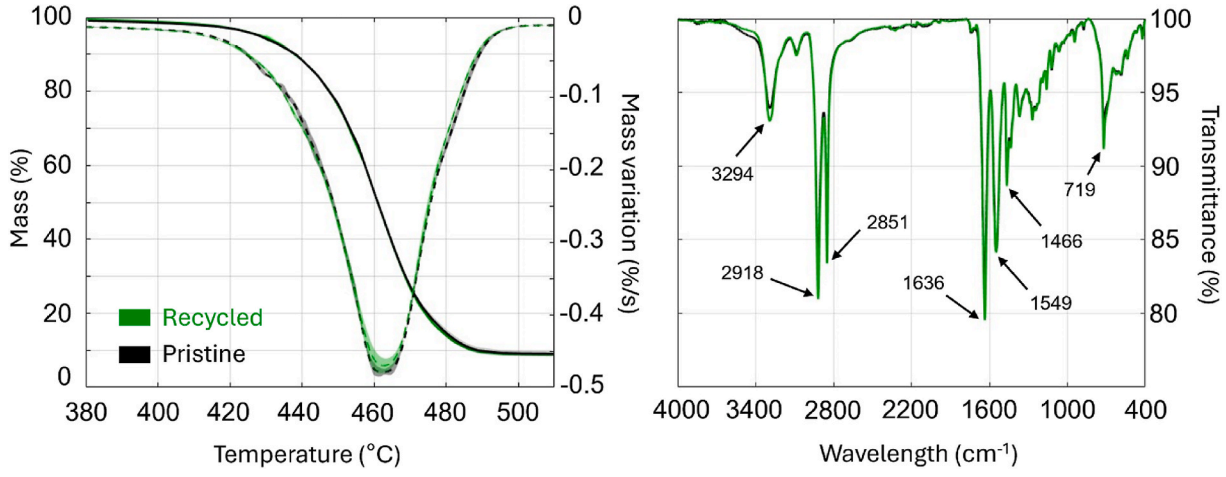

Fig. 8. TGA (left image) and ATR–FTIR (right image) results.

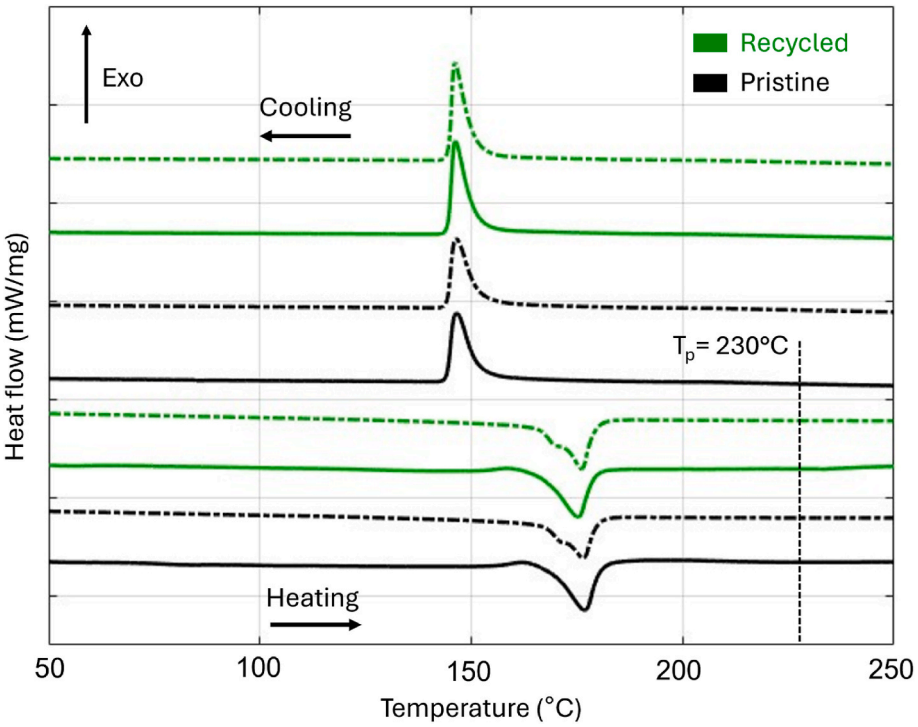

Fig. 9. Graph of the DSC (Differential Scanning Calorimetry) analyses.

Table 1
DSC data for pristine and recycled material.

	1st cycle		2nd cycle	
	Pristine	Recycled	Pristine	Recycled
T_m (°C)	177.0 ± 0.2	175.3 ± 0.1	176.6 ± 0.1	176.2 ± 0.2
ΔH_m (J/g))	47.8 ± 0.6	49.4 ± 2.4	36.9 ± 0.8	47.5 ± 1.6
χ_c (%))	25.0 ± 0.5	25.7 ± 1.4	–	–
T_c (°C))	153.4 ± 0.8	153.8 ± 0.1	153.3 ± 0.8	153.6 ± 0.3
ΔH_c (J/g))	47.2 ± 2.8	60.0 ± 4.7	47.4 ± 2.8	59.6 ± 4.3

carbon fibers. Two melting peaks were observed in the second heating run, explained by a melting-recrystallization process induced by the carbon fibers inside the PA12 matrix. Furthermore, the temperature differences between the two samples are reduced and become almost negligible (176.6 °C and 176.2 °C). Given that, in the second cycle, the sample size is likely similar between the two samples due to prior melting and recrystallization; it supports the assumption that the temperature difference observed in the first cycle is due to variations in sample size. The melting enthalpy in the second cycle is nearly the same as the first cycle for the recycled material (47.5 ± 1.6 J/g and 49.4 ± 2.4 J/g) but is significantly lower for the pristine material (36.9 ± 0.8 J/g and 47.8 ± 0.6 J/g). This discrepancy is a result of the lower crystallization enthalpy recorded for the pristine material. In terms of crystallization during the second cycle, no differences in temperature and enthalpy are observed compared to the first cycle, with the crystallization enthalpy of the pristine material remaining much lower than that of the recycled material (47.4 ± 2.8 J/g vs 59.6 ± 4.3 J/g).

3.2. Mechanical characterization results

In this section, the results of the mechanical characterization analysis are presented for both dogbone and tubular specimens, printed using FGF with pristine and recycled material as well as FFF with pristine filament. The dogbone focuses on the maximum achievable strength, while the tubular specimens assess layer adhesion. The results of the tensile tests are analyzed to evaluate elastic moduli, elongations at break, and maximum stresses of the materials investigated. A total of 5 dogbone and 5 tubular specimens are used for each material. Fig. 10 shows the results of the tensile tests. The continuous green lines represent results obtained by FGF specimens printed with recycled material, the continuous black lines represent results obtained by FGF specimens printed with pristine material, and the dashed black lines represent results obtained by FFF specimens printed with pristine material.

The results of the tensile tests are summarized in Table 2, which shows the elastic modulus, maximum stress, and maximum strain for the three materials analyzed. Comparable results for the dogbone specimens are found in the literature [50–52]. For all the materials analyzed, a noticeable difference is observed between the dogbone and tubular specimens in terms of mechanical properties. This finding aligns with previous results in the literature and highlights the strong anisotropy characteristic of 3D-printed materials [36,53–55]. Comparing the results for dogbone and tubular specimens, it can be seen that tubular specimens exhibit a more remarkable difference across the different materials tested. The microstructure of the FFF tubular specimen differs markedly from that of the FGF specimens, while this distinction is less pronounced in dogbone specimens. The FFF tubular specimens show a porous structure, with evident air gaps that compromise the geometry of the thin wall. Conversely, FFF dogbone specimens resemble the FGF specimens in terms of geometry, but they show more pronounced porosity. As a reference, Chisena et al. [56] investigated the porosity of 3D-printed parts realized with a short carbon fiber reinforced PA12, observing values up to 9.8 % of porosity in FFF specimens. The value of porosity not only depends on the fiber content and the printing parameters but also on the printed geometry, as observed in the present study.

Tensile tests conducted on both dogbone and tubular specimens highlight the superior mechanical performance of the recycled material. Tubular recycled FGF specimens are more brittle and slightly weaker than their pristine counterpart, meaning that inclusions can cause premature failure especially when dealing with very thin structures. Even

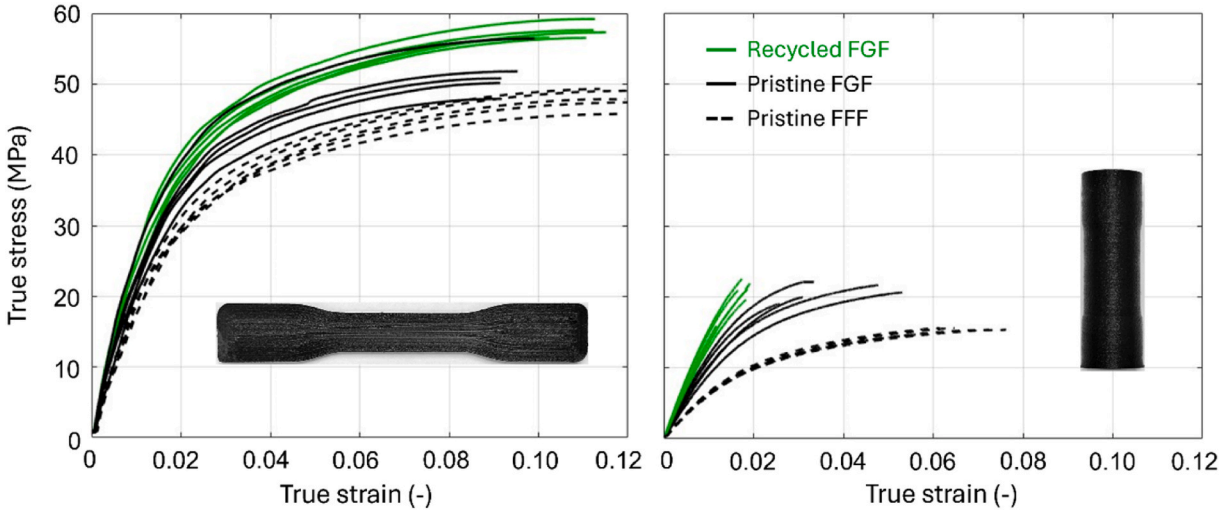

Fig. 10. True stress-true strain curves of the tensile tests on dogbone (left image) and tubular (right image) specimens.

Table 2
Summary of mean values of elastic moduli, maximum stresses, and maximum strains obtained. Standard deviation values are reported in brackets.

	Dogbone specimens			Tubular specimens		
	E (MPa)	σ_{max} (MPa)	ε_{max}	E (MPa)	σ_{max} (MPa)	ε_{max}
Recycled FGF)	2782 (230)	55.5 (0.6)	0.111 (0.005)	1459 (134)	20.1 (3.7)	0.017 (0.002)
Pristine FGF)	2626 (231)	50.6 (2.41)	0.094 (0.004)	1251 (179)	20.6 (1.6)	0.044 (0.015)
Pristine FFF	1946 (155)	46.4 (0.2)	0.119 (0.003)	682 (13)	15.2 (0.5)	0.067 (0.010)

very small inclusions can prevent the wall continuity and can act as a starting point for ruptures. The same considerations do not hold for the dogbone specimens, where the effect of inclusions is mitigated, and the microstructure is more evidently denser in recycled specimens rather than pristine ones. In terms of both elastic modulus and maximum stress, the recycled material outperforms (or is comparable with) the pristine material. The improvement of mechanical properties of recycled parts has already been observed in the literature. Previous studies by Walker et al. [14] also showed an improvement in the mechanical properties of recycled ABS tensile specimens. In their case, vertically printed parts resulted in higher mechanical properties due to the enhanced wettability of the recycled material, consequent to a reduction in fiber length. Nur-a-Tomal et al. [46] found almost identical mechanical properties when evaluating injection-molded PA12 over multiple recycling processes, demonstrating that, unlike other polymers, PA12 is more suitable for mechanical recycling. They observed a slight reduction in the maximum strength of dogbone specimens from 56 MPa to 52 MPa over 4 recycling processes. This means that the mechanical properties of PA12 remain relatively stable even after multiple recycling processes.

In the present study, the improvement observed in mechanical properties can be explained by the notable differences in microstructure, as observed in micro-CT scans. The recycled material exhibits higher density and fewer air pores, which are typical of the 3D printing process [57,58]. This could also be related to the composition of the feed material, characterized by a smaller particle size (as shown in Fig. 2a). Smaller particles inevitably promote a better printing process through a more complete homogenization of the melted material, thus favoring a more compact extruded filament. Air voids present in the feedstock materials (both pristine pellets and pristine filament) could also be transferred to the printed parts. To this end du Plessis et al. [59] investigated the quality of FFF commercial filaments via CT scans, observing porosities up to 2.7 %. They also observed a strict correlation between the quality of the filament to that of the 3D-printed part in terms of resultant porosity. In the case of the present study, air pores are observed while cutting the filament, thus the derived pellets may contain a small fraction of air that can increase porosity while printing. In the case of recycled flakes, air voids could be more effectively eliminated due to their thin nature, allowing for easier removal during the melting process. Additionally, the distribution and dispersion of short carbon fibers could benefit from a recycling process that involves a mechanical and physical transformation, as observed in Ref. [12]. Overall, the observed differences in mechanical properties are caused by the printing process, while the base material probably suffers little degradation which is not detected by the chemical analyses but is usually observed in the literature over multiple recycling processes [46]. Although the three feeding materials do not show significant chemical differences, relevant differences are observed in the final specimens, emphasizing the importance of understanding the printing process and the physical transformations materials undergo during 3D printing.

3.3. Case study results

As discussed in section 2.6, the case study aims to demonstrate the feasibility of 3D printing a functional component from recycled material. A comparison is made between the FGF printer using recycled material and the FFF printer using pristine filament. The results of the 3-point bending tests on the sandwich panels are presented in Fig. 11a:

Despite having the best mechanical properties, as discussed in the previous section, the recycled core shows the lowest energy absorption performance. This could be in contrast with the characterization results, but it can be explained by the modifications of the internal structure, implemented to obtain specimens with the same density. Another important aspect is that the actual mechanical properties of the recycled material could be overestimated due to the better realization of the test specimens. When printing the cores, the same microstructural observations made for the specimens could not hold, suggesting possible fluctuations in actual material properties due to the longer and more complicated printing process. As noted in section 2.6, the overall density

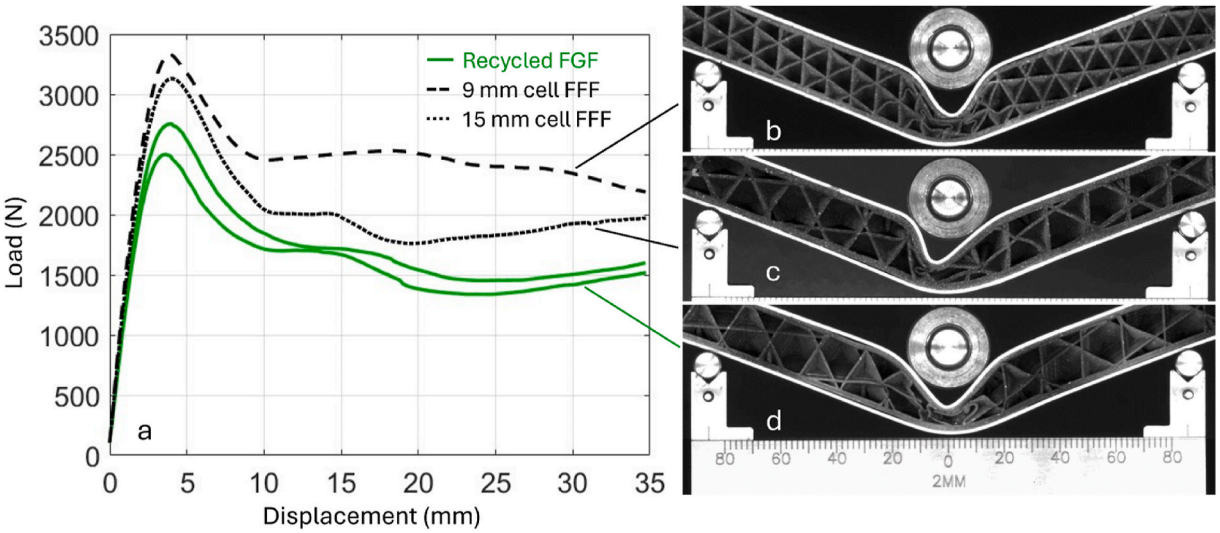

Fig. 11. Load-displacement curves of the 3-point bending tests on sandwich panels (a). Testing phases of FFF 9 mm cell core (b), FFF 15 mm cell core (c), and FGF core (d) are shown on the right side of the image.

of the cores is kept equal across the three configurations (recycled FGF, 9 mm cell FFF, and 15 mm cell FFF), necessitating adjustments to the wall thickness and the number of cells. It is known that cellular structures, such as those used in this study, mainly behave according to the bending and buckling of their internal walls [60]. The bending behavior of thin walls is greatly affected by their thickness, thus, even if the starting material is weaker, the bending performance is increased in FFF structures. Additionally, an increase in the number of cells greatly affects the energy absorption of the core by homogenizing the mechanical response and reducing the free length of the walls. In Fig. 11b, when a greater number of cells is involved, the load is more evenly distributed, and the overall behavior is less driven by individual collapses. Fig. 11c shows the behavior of the FFF 15 mm cell core and highlights this concept: the collapse is asymmetrical and driven by the first buckling of a cell wall. In contrast, Fig. 11d shows the bending behavior of the recycled FGF core, where a more diffused and pronounced collapse of cell walls is observed. The thinner walls of the recycled core favor the initial buckling of the cell walls, limiting the peak load the structure can sustain. As Netto et al. studied [61], when dealing with cellular structures with similar density, lower collapse forces and lower absorbed energies are observed for structures having larger cells or thinner walls. They also noted that by isolating the two factors, the effect of cell size is more prominent compared to that of the wall thickness. This can also be observed in the present work, where the major difference in terms of energy absorbed (herein considered the most important property for such structures) is obtained with the variation of the cell size. All cores experienced indentation failure due to the collapse of their internal structure. For this particular application, it is quite clear that the recycled material performs the lowest, likely due to its higher density. It is important to notice that for this specific application and load condition, the cubic structure with such density is not optimal. However, this structure resulted in easier prints compared to other infill structures, as observed by the authors in the early phase of the 3D printing setup. The relative dimensions of the cell compared to the whole structure localize the collapse, limit the involvement of other cells, and favor the indentation of the core. However, these limitations do not compromise the use of 3D-printed structures in similar applications, as demonstrated in previous works [62–64].

In this study, the sandwich panels are realized to test the fabrication process using recycled material and to compare it with the traditional FFF 3D printing method. The focus of the tests is on comparing the mechanical performance to demonstrate the feasibility of the recycling process and the potential for using a recycled cellular core as a lightweight reinforcement. In this context, the use of recycled material processes by FGF 3D printing proves to be a viable solution. Adjustments in terms of deposition strategy, infill geometry, and printing setup can further promote the mechanical performance of these components, as well as their diffusion.

In conclusion, the study of a functional component is necessary to effectively assess the feasibility of the recycling process via 3D printing technologies. If limited to standard test samples, considerations about the results of the longer and more complicated 3D printing process are not possible. However, in 3D printing, results should be always weighed on the scale of the printing process, suggesting that multi-scale studies are more reliable in this field. In this sense, the present work offers a wider spectrum of analysis with respect to similar works found in the literature, comparing the material's performance on a multi-scale level. The results of the case study prove novel findings about the behavior of 3D-printed materials at different dimensional scales of operation.

4. Summary and conclusions

In this work, a multi-disciplinary framework for recycling and 3D printing of thermoplastic short fiber-reinforced polymers is presented, from preliminary analyses to a final case study. Starting from a carbon short fiber-reinforced polyamide, both pristine and recycled materials are compared across two different levels. Two 3D printers are used to realize tensile specimens for a comparison between FFF and FGF 3D printing processes. Two types of tensile specimens are produced to analyze the degree of anisotropy under different printing and material conditions. Dogbone specimens are realized with a 0° raster angle to focus on material properties rather than microstructure, thereby maximizing the mechanical response. To avoid typical failures in the fillet regions, the G-code of the dogbone specimens is modified to employ a specific nozzle path which minimizes defects and abrupt direction changes. Tubular specimens are designed to analyze layer adhesion without the influence of raster angle, utilizing circular repeated patterns with a single pass for the nozzle path. Both specimens are thoroughly analyzed using micro-CT scans, revealing different microstructures based on both the material and the 3D printer used. TGA and ATR-FTIR analyses reveal no significant differences between recycled and pristine materials, indicating that the recycled material shows no notable alterations from its previous usage history. DSC analyses show slight differences associated with melting and crystallization enthalpies in heating and cooling cycles, while practically no difference is observed in characteristic temperatures. However, these dissimilarities do not

transpose into significantly different mechanical properties. Tensile tests demonstrate the appropriateness of the newly designed specimens, suggesting the potential for a new standardization based on G-code. The importance of the nozzle path has been demonstrated in previous studies, highlighting the need for a common procedure to realize specimens with 3D printing techniques. The mechanical tests reflect the observations of the micro-CT scans, attributing major differences in mechanical properties to microstructure. A case study is also presented to demonstrate the feasibility of the 3D printing process with recycled material: a sandwich panel with a 3D-printed core. Here, FFF 3D printing of pristine material is compared with FGF 3D printing of recycled material, with appropriate adjustments made to obtain consistent results in terms of energy absorption. The comparison indicates that while the pristine FFF material exhibits lower mechanical properties, it performs better in terms of energy absorption because of its architecture.

From the present study the following conclusions can be drawn:

- Geometry alone does not allow consistent results across different studies; greater attention must be paid to the standardization of the G-code. In particular, for a 0° raster angle, a modified G-code is necessary to avoid defects in the fillet regions.
- The microstructure of the specimens must be investigated due to the varying natures of different 3D printing processes. Significant microstructural differences can be observed even among namely identically processed 3D-printed materials.
- TGA and ATR-FTIR exclude relevant chemical and physical alterations of the molecular chains of the polymeric matrix. The DSC analysis excludes relevant differences between pristine and recycled materials regarding the 3D printing process, as confirmed by the equivalence of the characteristic melting temperatures and degree of crystallinity.
- In the case of FGF 3D printing, a carbon short fiber-reinforced polyamide is proven to be suitable for recycling, maintaining comparable mechanical properties to pristine material after one recycling cycle.
- Recycled material proves effective for large components, such as sandwich panel cores. However, the performance of these components is influenced by the internal structure of the cellular 3D-printed material, with the recycled core having a penalizing structure due to its higher density. The recycled core exhibits lower energy absorption capabilities, though this does not compromise its overall mechanical properties.
- FGF 3D printing is an efficient and straightforward method to process recycled polymers and future work should focus on its potential to reduce and manage plastic waste. A simple mechanical recycling process can be used to generate new feedstock, potentially with preliminary treatments in the case of more complex waste.

Future research should explore multiple recycling processes to assess probable polymeric matrix degradation after repeated melting cycles, possibly counterbalancing this with the addition of pristine material. The range of analyzed materials, characterized by different fillers and polymeric matrices, should be expanded to evaluate the suitability of FGF printing as a tool for plastic waste management. Additionally, a real-world case study should be conducted to account for mixed waste, in which preliminary sorting and treatment are necessary.

CRediT authorship contribution statement

Francesco Bandinelli: Writing – review & editing, Writing – original draft, Visualization, Validation, Software, Methodology, Investigation, Formal analysis, Data curation, Conceptualization. **Edoardo Tito:** Writing – review & editing, Writing – original draft, Validation, Methodology, Investigation, Formal analysis, Data curation, Conceptualization. **Emmanuele Parisi:** Methodology, Investigation. **Lorenzo Peroni:** Visualization, Validation, Supervision, Resources, Project administration, Methodology, Investigation, Funding acquisition, Conceptualization. **Martina Scapin:** Writing – review & editing, Validation, Supervision, Resources, Project administration, Methodology, Investigation, Conceptualization.

Declaration of competing interest

The authors declare that they have no known competing financial interests or personal relationships that could have appeared to influence the work reported in this paper.

Acknowledgments

The authors would like to thank FiberForce for providing the printing material and Ana Paula Pagnoncelli for her help in experimental activities on micro-CT scans. The research used the equipment of J-Tech and DYNLab Laboratory at Politecnico di Torino co-funded by POR FESR Piemonte 2014–2020.

Data availability

Data will be made available on request.

References

[1] OECD. Economic outlook. https://www.oecd.org/en/topics/economic-outlook.html. [Accessed 12 July 2024].
[2] Our world in data, FAQs on plastics. https://ourworldindata.org/faq-on-plastics. [Accessed 12 July 2024].
[3] UN environment programme. Annual report. https://www.unep.org/resources/annual-report-2023. [Accessed 13 July 2024]. 2023.
[4] Al-Salem SM, Lettieri P, Baeyens J. Recycling and recovery routes of plastic solid waste (PSW): a review. Waste Manag 2009;29(10):2625–43. https://doi.org/10.1016/j.wasman.2009.06.004.
[5] Mangold H, von Vacano B. The frontier of plastics recycling: rethinking waste as a resource for high-value applications. Macromol Chem Phys 2022;223(13):1–17. https://doi.org/10.1002/macp.202100488.
[6] Colorado HA, Velásquez EIG, Monteiro SN. Sustainability of additive manufacturing: the circular economy of materials and environmental perspectives. J Mater Res Technol 2020;9(4):8221–34. https://doi.org/10.1016/j.jmrt.2020.04.062.
[7] Hassan M, Mohanty AK, Misra M. 3D printing in upcycling plastic and biomass waste to sustainable polymer blends and composites: a review. Mater Des 2024;237(December 2023):112558. https://doi.org/10.1016/j.matdes.2023.112558.
[8] Mikula K, et al. 3D printing filament as a second life of waste plastics—a review. Environ Sci Pollut Res 2021;28(10):12321–33. https://doi.org/10.1007/s11356-020-10657-8.
[9] Rigon D, Ricotta M, Ardengo G, Meneghetti G. Static mechanical properties of virgin and recycled short glass fiber-reinforced polypropylene produced by pellet additive manufacturing. Fatig Fract Eng Mater Struct 2021;44(9):2554–69. https://doi.org/10.1111/ffe.13517.
[10] Romani A, Perusin L, Ciurnelli M, Levi M. Characterization of PLA feedstock after multiple recycling processes for large-format material extrusion additive manufacturing. Mater. Today Sustain. 2024;25(August 2023):100636. https://doi.org/10.1016/j.mtsust.2023.100636.
[11] Cruz Sanchez FA, Boudaoud H, Hoppe S, Camargo M. Polymer recycling in an open-source additive manufacturing context: mechanical issues. Addit Manuf 2017;17:87–105. https://doi.org/10.1016/j.addma.2017.05.013.
[12] Stan F, Stanciu NV, Fetecau C, Sandu IL. Mechanical recycling of low-density polyethylene/carbon nanotube composites and its effect on material properties. J Manuf Sci Eng 2019;141(9):1–7. https://doi.org/10.1115/1.4044101.
[13] Tian X, Liu Q T, Dilmurat A, Li D, Ziegmann G. Recycling and remanufacturing of 3D printed continuous carbon fiber reinforced PLA composites. J Clean Prod 2017;142:1609–18. https://doi.org/10.1016/j.jclepro.2016.11.139.
[14] Walker R, et al. Recycling of CF-ABS machining waste for large format additive manufacturing. Compos. Part B Eng. 2024;275:111291. https://doi.org/10.1016/j.compositesb.2024.111291.
[15] Woern AL, Byard DJ, Oakley RB, Fiedler MJ, Snabes SL, Pearce JM. Fused particle fabrication 3-D printing: recycled materials' optimization and mechanical properties. Materials 2018;11(8). https://doi.org/10.3390/ma11081413.
[16] Wu J, Zhang K, Yang D. Material extrusion additive manufacturing of recycled discontinuous carbon fibre reinforced thermoplastic composites with different fibre lengths: through-process microstructural evolution and mechanical property loss. Addit Manuf 2023;78(April):103839. https://doi.org/10.1016/j.addma.2023.103839.
[17] Anderson I. Mechanical properties of specimens 3D printed with virgin and recycled polylactic acid. 3D Print Addit Manuf 2017;4(2):110–5. https://doi.org/10.1089/3dp.2016.0054.

[18] Su N, Pierce RS, Rudd C, Liu X. Comprehensive investigation of reclaimed carbon fibre reinforced polyamide (rCF/PA) filaments and FDM printed composites. Compos. Part B Eng. 2022;233(January):109646. https://doi.org/10.1016/j.compositesb.2022.109646.
[19] Ma W, Dong Q, Zhao H, Li X, Xiong L, Hu N. Mechanics-guided manufacturing optimization framework to enhance the strength of architected lattice made from recycled plastic wastes. Addit Manuf 2024;81(December 2023):103997. https://doi.org/10.1016/j.addma.2024.103997.
[20] Alexandre A, Cruz Sanchez FA, Boudaoud H, Camargo M, Pearce JM. Mechanical properties of direct waste printing of polylactic acid with universal pellets extruder: comparison to fused filament fabrication on open-source desktop three-dimensional printers. 3D Print Addit Manuf 2020;7(5):237–47. https://doi.org/10.1089/3dp.2019.0195.
[21] Copenhaver K, et al. Recyclability of additively manufactured bio-based composites. Compos. Part B Eng. 2023;255(August 2022):110617. https://doi.org/10.1016/j.compositesb.2023.110617.
[22] Korey M, et al. Recycling polymer composite granulate/regrind using big area additive manufacturing. Compos. Part B Eng. 2023;256(October 2022):110652. https://doi.org/10.1016/j.compositesb.2023.110652.
[23] Justino Netto JM, Idogava HT, Frezzatto Santos LE, Silveira Z de C, Romio P, Alves JL. Screw-assisted 3D printing with granulated materials: a systematic review. Int J Adv Manuf Technol 2021;115(9–10):2711–27. https://doi.org/10.1007/s00170-021-07365-z.
[24] Pignatelli F, Percoco G. An application- and market-oriented review on large format additive manufacturing, focusing on polymer pellet-based 3D printing. Prog. Addit. Manuf. 2022;7(6):1363–77. https://doi.org/10.1007/s40964-022-00309-3.
[25] Cruz Sanchez FA, Boudaoud H, Camargo M, Pearce JM. Plastic recycling in additive manufacturing: a systematic literature review and opportunities for the circular economy. J Clean Prod 2020;264:121602. https://doi.org/10.1016/j.jclepro.2020.121602.
[26] Liu H, Gong K, Portela A, Cao Z, Dunbar R, Chen Y. Granule-based material extrusion is comparable to filament-based material extrusion in terms of mechanical performances of printed PLA parts: a comprehensive investigation. Addit Manuf 2023;75. https://doi.org/10.1016/j.addma.2023.103744.
[27] Reich MJ, Woern AL, Tanikella NG, Pearce JM. Mechanical properties and applications of recycled polycarbonate particle material extrusion-based additive manufacturing. Materials May 2019;12(10):1642. https://doi.org/10.3390/ma12101642.
[28] Sanders B, Cant E, Amel H, Jenkins M. The effect of physical aging and degradation on the Re-use of polyamide 12 in powder bed fusion. Polymers 2022;14(13). https://doi.org/10.3390/polym14132682.
[29] Su D, Yang J, Liu S, Ren L, Qin S. Preparation of polyamide 12 powder for additive manufacturing applications via thermally induced phase separation. E-Polymers 2022;22(1):553–65. https://doi.org/10.1515/epoly-2022-0050.
[30] El Magri A, Bencaid SE, Vanaei HR, Vaudreuil S. Effects of laser power and hatch orientation on final properties of PA12 parts produced by selective laser sintering. Polymers 2022;14(17). https://doi.org/10.3390/polym14173674.
[31] Bahrami M, Abenojar J, Martínez MA. Comparative characterization of hot-pressed polyamide 11 and 12: mechanical, thermal and durability properties. Polymers (Basel) 2021;13(20):1–21. https://doi.org/10.3390/polym13203553.
[32] Ma N, et al. Crystal transition and thermal behavior of Nylon 12. E-Polymers 2020;20(1):346–52. https://doi.org/10.1515/epoly-2020-0039.
[33] Mistry BD. A handbook of spectroscopic data 2009;36(2).
[34] Hui D, Goodridge RD, Scotchford CA, Grant DM. Laser sintering of nano-hydroxyapatite coated polyamide 12 powders. Addit Manuf 2018;22(March 2017):560–70. https://doi.org/10.1016/j.addma.2018.05.045.
[35] Han J, Cao Z, Gao W. Remarkable sorption properties of polyamide 12 microspheres for a broad-spectrum antibacterial (triclosan) in water. J Mater Chem A 2013;1(16):4941–4. https://doi.org/10.1039/c3ta00090g.
[36] Ziemian C, Sharma M, Ziemi S. Anisotropic mechanical properties of ABS parts fabricated by fused deposition modelling. Mechanical Engineering February 2018, 2012.
[37] Calignano F, Lorusso M, Roppolo I, Minetola P. Investigation of the mechanical properties of a carbon fibre-reinforced nylon filament for 3d printing. Machines Sep. 2020;8(3):1–13. https://doi.org/10.3390/machines8030052.
[38] Bandinelli F, Scapin M, Peroni L. Effects of anisotropy and infill pattern on compression properties of 3D printed CFRP: mechanical analysis and elasto-plastic finite element modelling. Rapid Prototyp J 2024;30(11):142–58. https://doi.org/10.1108/RPJ-11-2023-0385.
[39] Phillips C, Kortschot M, Azhari F. Towards standardizing the preparation of test specimens made with material extrusion: review of current techniques for tensile testing. Addit Manuf 2022;58(July):103050. https://doi.org/10.1016/j.addma.2022.103050.
[40] Sola A, et al. Open challenges in tensile testing of additively manufactured polymers: a literature survey and a case study in fused filament fabrication. Polym Test 2023;117(September 2022):107859. https://doi.org/10.1016/j.polymertesting.2022.107859.
[41] Kim SK, Kazmer DO, Colon AR, Coogan TJ, Peterson AM. Non-Newtonian modeling of contact pressure in fused filament fabrication. J. Rheol. (N. Y. N. Y). 2021;65(1):27–42. https://doi.org/10.1122/8.0000052.
[42] Bochnia J, Blasiak M, Kozior T. A comparative study of the mechanical properties of fdm 3d prints made of pla and carbon fiber-reinforced pla for thin-walled applications. Materials 2021;14(22). https://doi.org/10.3390/ma14227062.
[43] Bandinelli F, Peroni L, Scapin M. Experimental investigation of 3D printed infill structures for crash absorbing applications. Mater Lett 2024;354(October 2023):135373. https://doi.org/10.1016/j.matlet.2023.135373.
[44] Slapnik J, Pulko I, Rudolf R, Anžel I, Brunčko M. Fused filament fabrication of Nd-Fe-B bonded magnets: comparison of PA12 and TPU matrices. Addit Manuf 2021;38. https://doi.org/10.1016/j.addma.2020.101745.
[45] Dencheva N, Denchev Z, Oliveira MJ, Funari SS. Crystallization behavior of poly (ε-caprolactone)/layered double hydroxide nanocomposites. J Appl Polym Sci 2006;103(5):2242–52. https://doi.org/10.1002/app.25250.
[46] Nur-a-Tomal MS, Pahlevani F, Handoko W, Cholake ST, Sahajwalla V. Effect of cyclic reprocessing on nylon 12 under injection molding: working toward more efficient recycling of plastic waste. Materials Today Sustainability March 2021;11–12. https://doi.org/10.1016/j.mtsust.2020.100056.
[47] Vadori R, Mohanty AK, Misra M. The effect of mold temperature on the performance of injection molded Poly(lactic acid)-based bioplastic. Macromol Mater Eng 2013;298(9):981–90. https://doi.org/10.1002/mame.201200274.
[48] Weinmann S, Bonten C. Recycling of pa12 powder for selective laser sintering. AIP Conf Proc 2020;2289(September). https://doi.org/10.1063/5.0029945.
[49] Wang Lu, Kiziltas Alper, Mielewski Deborah F, Lee Ellen C, Gardner Douglas J. Closed-loop recycling of polyamide 12 powder from selective laser sintering into sustainable composites. J Clean Prod September 2018;195:765–72. https://doi.org/10.1016/j.jclepro.2018.05.235.
[50] Pejkowski Ł, Seyda J, Nowicki K, Mrozik D. Mechanical performance of non-reinforced, carbon fiber reinforced and glass bubbles reinforced 3D printed PA12 polyamide. Polym Test November 2022;118:1–11. https://doi.org/10.1016/j.polymertesting.2022.107891. 2023.
[51] Liao G, et al. Properties of oriented carbon fiber/polyamide 12 composite parts fabricated by fused deposition modeling. Mater Des 2018;139:283–92. https://doi.org/10.1016/j.matdes.2017.11.027.
[52] Le Gentil T, Therriault D, Kerbrat O. A comprehensive methodology to support decision-making for additive manufacturing of short carbon-fiber reinforced polyamide 12 from energy, cost and mechanical perspectives. Int J Adv Manuf Technol 2024;131(2):611–22. https://doi.org/10.1007/s00170-023-11161-2.
[53] Bandinelli F, Peroni L, Morena A. Elasto-plastic mechanical modeling of fused deposition 3D printing materials. Polymers (Basel). 2023;15(1). https://doi.org/10.3390/polym15010234.
[54] Athale M, Park T, Hahnlen R, Pourboghrat F. Experimental characterization and finite element simulation of FDM 3D printed polymer composite tooling for sheet metal stamping. Int J Adv Manuf Technol 2022;121(9–10):6973–89. https://doi.org/10.1007/s00170-022-09801-0.
[55] Zeybek MK, Güden M, Taşdemirci A. The effect of strain rate on the compression behavior of additively manufactured short carbon fiber-reinforced polyamide composites with different layer heights, infill patterns, and built angles. J Mater Eng Perform 2023;14. https://doi.org/10.1007/s11665-023-07918-1.
[56] Chisena Robert S, Engstrom Sophia Marina, Shih Albert J. Computed tomography evaluation of the porosity and fiber orientation in a short carbon fiber material extrusion filament and part. Addit Manuf August 2020;34. https://doi.org/10.1016/j.addma.2020.101189.
[57] Wickramasinghe S, Do T, Tran P. FDM-based 3D printing of polymer and associated composite : a review on mechanical properties. 2020.
[58] Kim HC, Tu R, Sodano HA. Room temperature 3D printing of high-temperature engineering polymer and its nanocomposites with porosity control for multifunctional structures. Compos. Part B Eng. 2024;279(April):111444. https://doi.org/10.1016/j.compositesb.2024.111444.
[59] Du Plessis A, Le Roux SG, Steyn F. Quality investigation of 3D printer filament using laboratory X-ray tomography. 3D Print Addit Manuf 2016;3(4):262–7. https://doi.org/10.1089/3dp.2016.0011.
[60] Lakes RS. Cellular solids. J Biomech 1989;22(4):397. https://doi.org/10.1016/0021-9290(89)90056-0.
[61] Netto JJ, Sardinha M, Leite M. Influence of the cell size and wall thickness on the compressive behaviour of fused filament fabricated PLA gyroid structures. Mech Mater August 2024;195. https://doi.org/10.1016/j.mechmat.2024.105051.
[62] Cao X, et al. Compression experiment and numerical evaluation on mechanical responses of the lattice structures with stochastic geometric defects originated from additive-manufacturing. Compos. Part B Eng. 2020;194(December 2019):108030. https://doi.org/10.1016/j.compositesb.2020.108030.
[63] Higuera S, Miralbes R, Ranz D. Mechanical properties and energy–absorption capabilities of thermoplastic sheet gyroid structures. Mech Adv Mater Struct 2022;29(25):4110–24. https://doi.org/10.1080/15376494.2021.1919803.
[64] Yazdani Sarvestani H, Akbarzadeh AH, Mirbolghasemi A, Hermenean K. 3D printed meta-sandwich structures: failure mechanism, energy absorption and multi-hit capability. Mater Des 2018;160:179–93. https://doi.org/10.1016/j.matdes.2018.08.061.